Supplementary Information for

Magnetically locked Janus particle clusters with orientation-dependent motion in AC electric fields

Jin Gyun Lee[†], Cooper P. Thome[†], Zoe A. Cruse, Arkava Ganguly, Ankur Gupta,

C. Wyatt Shields IV[*]

Department of Chemical and Biological Engineering, University of Colorado Boulder,

Boulder, CO 80303, United States

[†]**Equal contribution**

***Corresponding author.** C. Wyatt Shields IV: Department of Chemical and Biological Engineering; Biomedical Engineering Program; University of Colorado Boulder; Boulder, CO 80303, United States. Email: Charles.Shields@colorado.edu

The PDF file includes:
Figures S1 to S7
Legends for Movies S1 to S5
References

Other Supporting Information for this manuscript include the following:
Movies S1 to S5

Coplanar electrode propulsion chamber. The propulsion chamber utilized in this study is shown in Fig. S1. To operate the chamber, a sample of particle clusters was placed between the two gold electrodes within a drawn hydrophobic boundary and two PTFE tape spacers. After placing a coverslip on top of the PTFE spacers, the particle sample spread to the boarders of the hydrophobic boundary. An electric field was generated by applying an AC square wave from a function generator attached to the device by leads and copper tape.

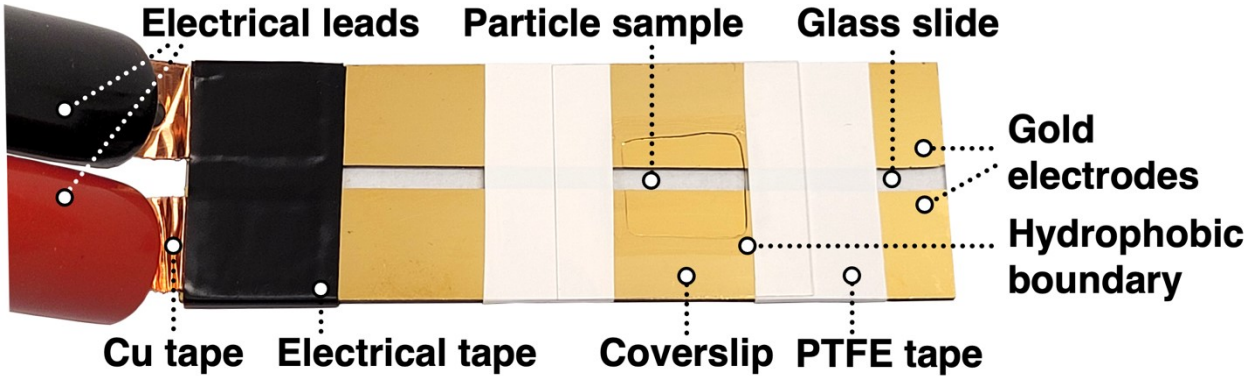

Fig. S1. Image of the coplanar electrode propulsion chamber used to apply the AC electric field to particle samples.

Alignment of Janus clusters and assembly of Janus particles upon applying an AC electric field. As shown in Fig. 1C-E of the main text, non-magnetic Janus particle clusters can cluster and align by the applied field due to DEP, resulting in arrested motion. Notably, this phenomenon can also occur, though infrequently, for magnetic Janus particle clusters (Fig. S2).

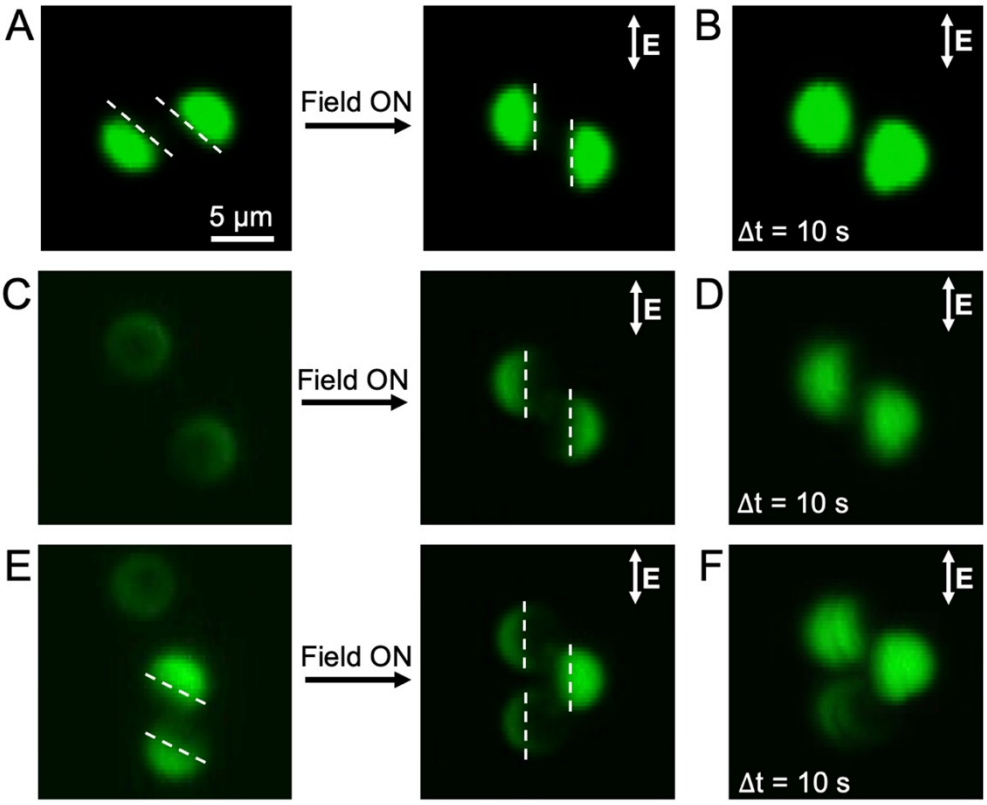

Fig. S2. Fluorescent microscope images of magnetic Janus particles of staggered chains exhibiting no motion in an AC electric field. A. Images showing the alignment of a pre-assembled magnetic Janus particle dimer upon application of an electric field. B. Superimposed microscope images showing a Janus particle dimer in (A) with no motion in an electric field. C. Images showing the assembly of Janus particles into a staggered chain upon the application of an electric field. D. Superimposed microscope images showing a Janus particle dimer in (C) with no motion in an electric field. E. Images showing the assembly of a Janus particle and a Janus dimer into a staggered chain upon the application of an electric field. F. Superimposed microscope images showing a Janus trimer in (E) with no motion in an electric field.

Inhibited motion of a Janus particle dimer. Among the regimes of motions found in the presented system, several clusters resulted in inhibited (nil) motion (Fig. S3).

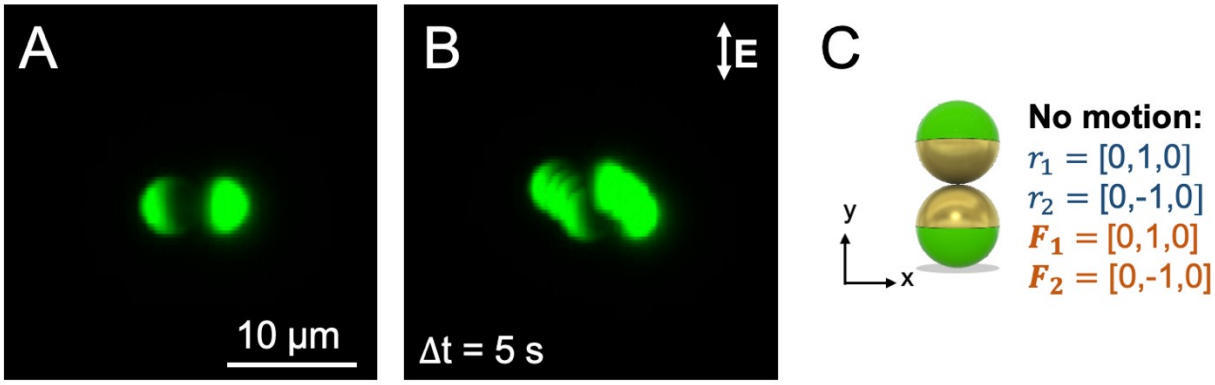

Fig. S3. Janus particle cluster exhibiting no motion in an AC electric field. A. Fluorescent microscope image of two Janus particles facing each other in a dimeric cluster. B. Superimposed fluorescent microscope images showing a Janus particle dimer in (A) with no motion in an AC electric field. The slight motion of the dimer is attributed to bulk fluid flow in the propulsion chamber. C. Schematic illustration of the configuration of the dimer showing no motion and the extracted approximate vectors using a rigid bead model showing no motion.

Theoretical framework. To gain a mechanistic understanding of the experimentally realized particle motion, we examined the motion of dimers using a mobility formulation. The dimer configurations were seen to depend on two geometric parameters: (i) the position of the point-of-contact between the two spheres; and (ii) the relative positions of the metallic patches on the particles (Fig. S4).

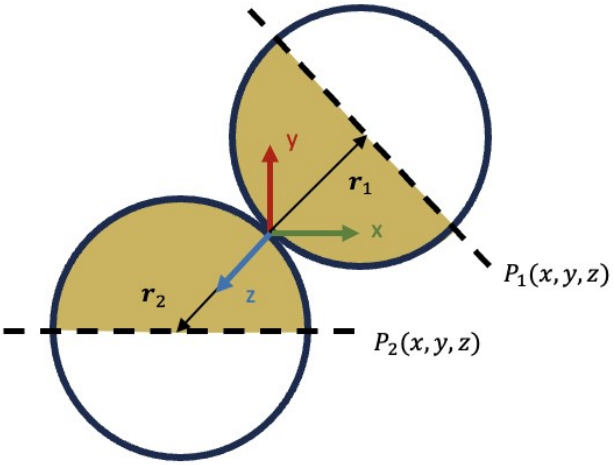

Fig. S4. Schematic illustration of the geometry of a general dimer configuration. The point-of-contact between the particles is the origin of the local coordinate system. The position vectors of the centers of the two spherical particles are r_1 and r_2, respectively. The metallic patches are specified using 3D planar functions $p_1(x, y, z)$ and $p_2(x, y, z)$ such that the metallic surfaces are always in contact with each other.

The configurations of particles within the dimers are obtained by different combinations of r_1, r_2, $p_1(x, y, z)$, $p_2(x, y, z)$, described in Fig. S3 and the corresponding caption. The hydrodynamic properties of these rigid dimer configurations are obtained by implementation of the Generalized Rotne-Prager-Yamakawa method on these dimeric systems [1]. The length scale of these dimers is small, and it is appropriate to describe the flow around these particles using Stokes and continuity equations,

$$\eta\nabla^2 v - \nabla p = 0, \qquad (1)$$

and

$$\nabla \cdot v = 0, \tag{2}$$

where v is the fluid velocity, p is the pressure, and η is the fluid viscosity. The force and velocity moments on the dimer can be represented in terms of their velocity moments due to the linearity of Eqs. (1) and (2)

$$\begin{bmatrix} F \\ T \end{bmatrix} = -\begin{bmatrix} \zeta^{tt} & \zeta^{tr} \\ \zeta^{rt} & \zeta^{rr} \end{bmatrix} \begin{bmatrix} U \\ \Omega \end{bmatrix}. \tag{3}$$

The force $F = [F_1\, F_2]$ and torque $T = [T_1\, T_2]$ are 6-dimensional vectors, where F_1, T_1, F_2, T_2 are the force and torque on each of the two particles, respectively. The direction of F_1 and F_2 depends on both the position vectors $r_1$and r_2 and the orientation of the patches $p_1$and p_2. There are no external torques acting on the particle, $T_1 = T_2 = 0$. The translation and rotation velocities, U and Ω, are similarly written. An inversion in Eq. (3) gives us the mobility expression,

$$\begin{bmatrix} U \\ \Omega \end{bmatrix} = \begin{bmatrix} \mu^{tt} & \mu^{tr} \\ \mu^{rt} & \mu^{rr} \end{bmatrix} \cdot \begin{bmatrix} F \\ T \end{bmatrix}, \tag{4}$$

by which U and Ω are obtained for a given F and T. In the absence of a magnetic field, when the particle is being propelled by an AC electric field, the dimers rotate as a rigid body. This allows us to rewrite the grand mobility expression in Eq. (4) to a mobility expression where the force, torque, and velocities are defined with respect to the center of mass of the particle,

$$\begin{bmatrix} U_c \\ \Omega_c \end{bmatrix} = \begin{bmatrix} m^{tt} & m^{tr} \\ m^{rt} & m^{rr} \end{bmatrix} \cdot \begin{bmatrix} F_c \\ T_c \end{bmatrix}. \tag{5}$$

The force and torque acting on the particle center of mass are obtained by addition of the individual F_i and T_i acting on the i^{th} particle, $F_c = \sum_i F_i$ and $T_c = \sum_i (T_i + r_i \times F_i)$. The detailed derivation of the mobility coefficients is given by a generalized version of the Roten-Prager-Yamakawa mobility expression [2,3] and can be found in Wajnryb et al. [4]. Equation (5) conveniently provides U_c and Ω_c for specific F_c and T_c through the mobility matrix m, which depends on the geometric configuration of the dimer. In the next sub-section, we provide a short outline of particle kinematics.

Particle kinematics

We consider that the driving force on the dimer is constant at a body frame of reference (e_x,e_y,e_z). Consequently, the rotation and translation velocity, U_c and Ω_c, are also in this body frame. To obtain the laboratory frame motion of the particle, the body frame unit vectors are evolved with time according to

$$\frac{de_i}{dt} = \Omega_c \times e_i, \quad i = x,y,z$$

$$\frac{dR_c}{dt} = U_c \tag{6}$$

where the unit vectors e_i, and the center-of-mass position are expressed in the laboratory reference frame. The expressions in Equation (6) can be written as a linear system of equations to obtain the body frame of reference and center of mass position with time

$$e_i(t+dt) = e_i(t) + \frac{de_i}{dt}\delta t$$

$$\begin{bmatrix} e_x(t+dt) \\ e_y(t+dt) \\ e_z(t+dt) \end{bmatrix} = R \begin{bmatrix} e_x \\ e_y \\ e_z \end{bmatrix}. \tag{7}$$

This resulting rotation matrix, ***R***, allows for the center-of-mass position to be rotated and translated to follow a path of motion within the body frame of reference. The respective particle and patch positions are further updated using the rotation matrix to adjust their position within the same reference frame.

$$r_{COM}(t+dt) = r_{COM}(t) + U \cdot R\, dt \tag{8}$$

Extended characterization of trochoidal and helical motions of Janus dimers in an AC electric field. To further examine the trochoidal and helical motions shown in Fig. 3B and C of the main text and evaluated in Fig. 3E and F, we evaluated trochoidal and helical cluster movement using time as a third dimension (Fig. S5 and S6). The oscillating behaviors in the X-direction of each trajectory over time are signatures of trochoidal and helical motions.

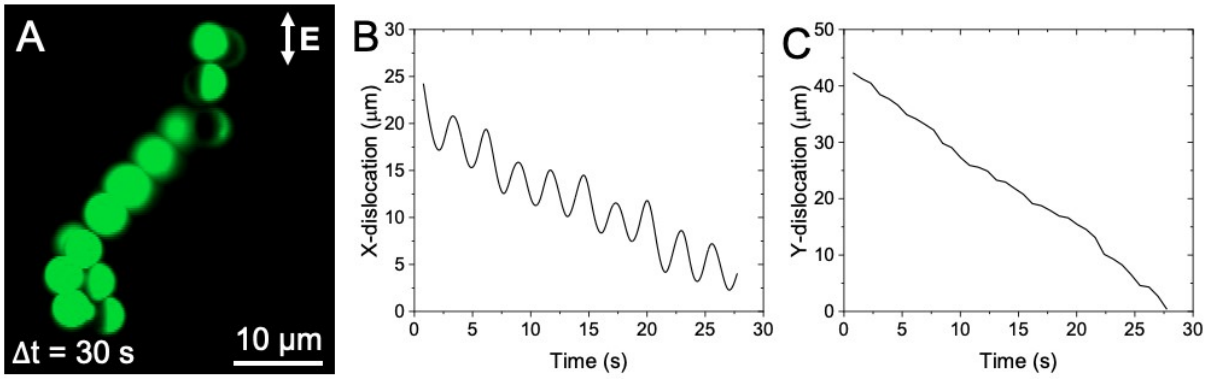

Fig. S5. Characterization of trochoidal motion of a Janus dimer in an AC electric field. A. Superimposed fluorescence image of a Janus dimer self-propelling with trochoidal motion in an AC electric field. B-C. Displacement of the Janus dimer displaying trochoidal motion in X- and Y-directions over time.

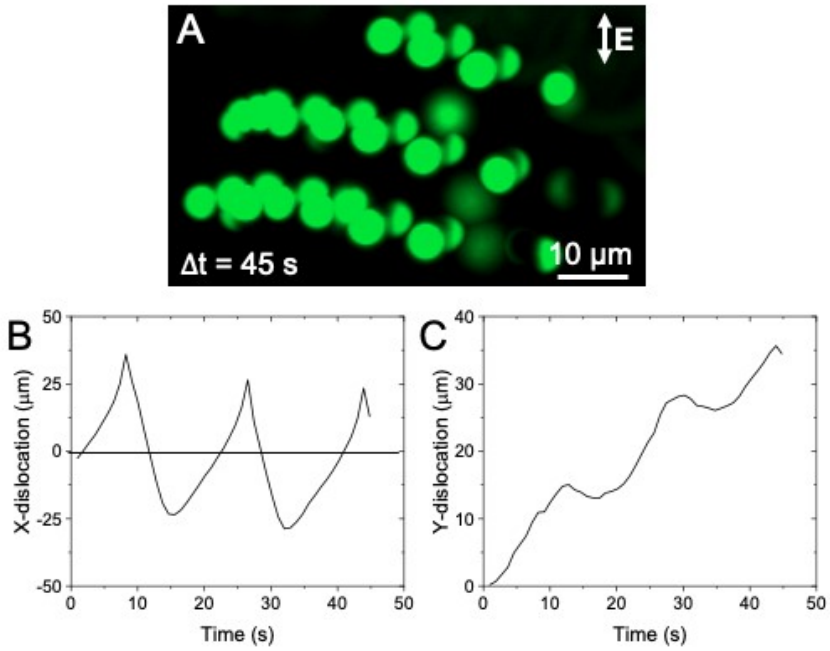

Fig. S6. Characterization of helical motion of a Janus dimer in an AC electric field. A. Superimposed fluorescence image of a Janus dimer self-propelling with helical motion in an AC electric field. B-C. Displacement of the Janus dimer displaying helical motion in X- and Y-directions over time.

Additional patchy particle fabrication details. Patchy particles were fabricated by glancing angle deposition of Cr, Co, and Au during electron-beam evaporation (Fig. S7).

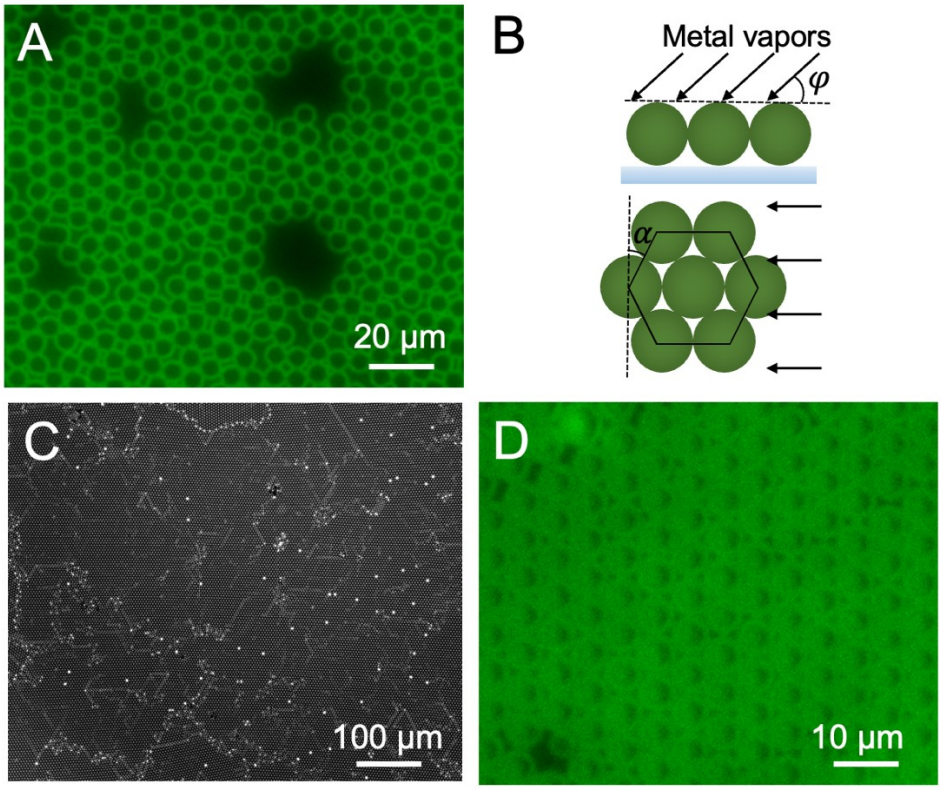

Fig. S7. Fabrication of patchy particles. A. Fluorescent microscope image showing polystyrene (PS) spheres in a submonolayer (diameter = 5.1 μm) assembled using a convective assembly method. B. Schematic illustration of glancing angle deposition of metal onto PS spheres. φ = angle of incident vapor beam, α = monolayer orientation angle. C. Bright-field microscope image showing a closed-pack monolayer of PS spheres assembled by Langmuir-Blodgett deposition. D. Fluorescent microscope image showing PS spheres with triangular patches on their surfaces ($\varphi = 10°$).

Supplementary Movies

Movie S1. Translational motion of a Janus dimer cluster.

Movie S2. Rotational motion of a Janus dimer cluster.

Movie S3. Trochoidal motion of a Janus dimer cluster.

Movie S4. Helical motion of a Janus dimer cluster.

Movie S5. Propulsion of a Janus-patchy dimer cluster and a Janus trimer.

References

1. Zuk, Pawel J., Bogdan Cichocki, and Piotr Szymczak. "GRPY: an accurate bead method for calculation of hydrodynamic properties of rigid biomacromolecules." *Biophysical Journal* 115.5 (2018): 782-800.
2. Yamakawa, Hiromi. "Transport properties of polymer chains in dilute solution: hydrodynamic interaction." *The Journal of Chemical Physics* 53.1 (1970): 436-443.
3. Rotne, Jens, and Stephen Prager. "Variational treatment of hydrodynamic interaction in polymers." *The Journal of Chemical Physics* 50.11 (1969): 4831-4837.
4. Wajnryb, Eligiusz, et al. “Generalization of the Rotne–Prager–Yamakawa Mobility and Shear Disturbance Tensors.” Journal of Fluid Mechanics, vol. 731, 2013, p. R3., doi:10.1017/jfm.2013.402.